THE JOURNAL OF PHYSICAL CHEMISTRY C
A JOURNAL OF THE AMERICAN CHEMICAL SOCIETY

pubs.acs.org/JPCC

Article

Exciton Polariton-Enhanced Photodimerization of Functionalized Tetracene

Richard Puro, Jonathan D. B. Van Schenck, Reid Center, Emma K. Holland, John E. Anthony, and Oksana Ostroverkhova*

Cite This: J. Phys. Chem. C 2021, 125, 27072−27083

Read Online

ACCESS | Metrics & More | Article Recommendations | Supporting Information

ABSTRACT: We explore the photodegradation mechanisms in functionalized tetracene (TIPS-Tc) films and how they are influenced by strong exciton−photon coupling in planar microcavities. We demonstrate that degradation of TIPS-Tc films exposed to air proceeds mainly through an oxygen-mediated pathway, assigned to endoperoxide (EPO) formation, whereas degradation in microcavities proceeds through oxygen-independent photodimerization. The aerobic and anaerobic decay mechanisms were found to differ in rate by more than two orders of magnitude. Both the EPO formation and photodimerization proceeded more efficiently in molecules in configurations favorable for the correlated triplet pair (TT) state formation (precursor to the singlet fission) and their immediate surroundings. For the photodimerization, an alkyne dimer is reported as one of the photoproducts, and its optical properties are presented. Strong coupling of TIPS-Tc to resonant microcavities enhanced the photodimerization quantum yield by a factor of 4.2, with the enhancement robust with respect to cavity detuning.

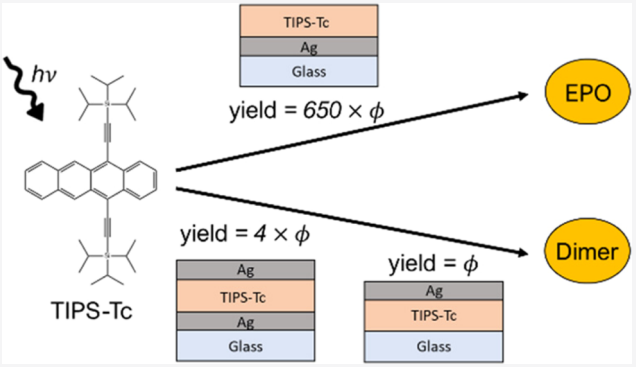

1. INTRODUCTION

Organic (opto)electronic materials have attracted attention because of their low cost, ease of fabrication, and tunable properties;[1] applications including thin-film transistors, solar cells, light-emitting diodes, and sensors have been demonstrated, and many of them are commercialized.[2] One of the main challenges in the commercialization of organic semiconductors is their low stability in the presence of light and oxygen, which results in degradation and device failure. Therefore, understanding of degradation mechanisms in high-performance organic semiconductors is of considerable importance.[2] Polariton chemistry, which utilizes strong light−matter interactions to control chemical reactions, is an emerging field of recent interest.[3−7] Both acceleration and inhibition of chemical reaction rates because of strong coupling of molecules to cavity photons, depending on the reaction, have been predicted theoretically,[8,9] and several reactions under strong coupling conditions, both in the ground[10,11] and in the excited[12,13] electronic states, have been studied experimentally. Effects of strong coupling on the photochemical reactions pertaining to the photostability of organic electronic materials have also been reported. For example, strong coupling between the J-aggregated organic dye and triangular silver nanoprisms resulted in up to a hundredfold reduction in the photobleaching rate in the dye molecules,[12] and a threefold stabilization factor was obtained because of coupling of a semiconducting polymer P3HT to a microcavity.[14] In both cases, the photodegradation process, mediated by the strong coupling, was related to triplet (T_1) state-mediated photo-oxidation.

Functionalized acenes have served as model systems for a variety of studies of exciton and charge carrier dynamics, and they are among the highest-performing organic semiconductors to date.[1] Strong exciton−photon coupling in various acene crystals and films placed in microcavities has also been observed,[15−18] and polariton lasing was demonstrated.[19] A representative of this class is 5,12-bis(triisopropylsilyl)ethynyl tetracene (TIPS-Tc, inset of Figure 1) which has been extensively studied as a singlet fission material.[20−22] (Singlet fission is a process of generating two triplet states from a singlet exciton, providing a route to boost the efficiency of organic solar cells.[23]) Similar to other acene derivatives,[15−18] TIPS-Tc films placed in microcavities exhibit polariton formation because of strong coupling of excitons in the TIPS-Tc to the cavity photon.[24] A notable drawback of using the TIPS-Tc derivative in devices, however, is that it is prone to a rapid photo-

Received: August 4, 2021
Revised: November 22, 2021
Published: December 5, 2021

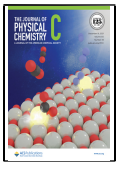

https://doi.org/10.1021/acs.jpcc.1c06881
J. Phys. Chem. C 2021, 125, 27072−27083

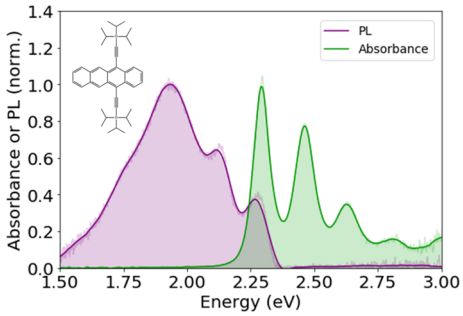

Figure 1. Absorption and PL spectra, normalized at their peak values, of pristine TIPS-Tc films used in our studies. The inset shows the molecular structure of TIPS-Tc.

degradation[25] under ambient conditions, which calls for investigation of underlying mechanisms. The ability of TIPS-Tc to form exciton polaritons in a microcavity presents an opportunity not only to explore technologically relevant photochemical reactions but also to determine whether they could be manipulated using polaritons.

In this paper, we examine the routes of photodegradation in TIPS-Tc films and establish how they are affected by the strong coupling of TIPS-Tc excitons to the cavity photons. We demonstrate the presence of both oxygen-mediated and oxygen-independent mechanisms of degradation, which proceed with rates differing by a factor of ∼650. For the oxygen-independent pathway, we identify an alkyne dimer as one of the major photoproducts and report on its optical properties. We observe an accelerated photodimerization in the presence of cavity polaritons, with the rate enhanced by a factor of ∼4 in resonant cavities and only slightly depending on the cavity detuning.

2. MATERIALS AND METHODS

2.1. Sample Preparation. TIPS-Tc films were spin cast from a 50 mM solution in toluene on a glass substrate which was partially covered with a 45 nm layer of Ag. The spin casting speed was varied to create films with thicknesses ranging between 95 and 140 nm, as measured using ellipsometry. All films were amorphous as confirmed by the X-ray diffraction. Three sample configurations were created on the same substrate: TIPS-Tc/Ag (45 nm)/glass (denoted "**B**" for the Ag on the "bottom"), Ag (45 nm)/TIPS-Tc/glass (denoted "**T**" for Ag on the "top"), and Ag (45 nm)/TIPS-Tc/Ag (45 nm)/glass (denoted "**C**" for "cavities"); schematics of **B** and **T** samples are shown in the insets of Figure 2a,b. The range of film thicknesses was chosen to create $\lambda/2$ microcavities with varying resonance frequencies, so that the cavity detuning Δ defined as $\Delta = E_0 - E_X$ (where E_0 is the cavity photon energy at normal incidence and E_X is the TIPS-Tc 0−0 exciton energy) is in the −328 to +126 meV range (Table 1). Details of fabrication and properties of samples studied are provided in the SI. **T** samples prepared on the same substrates as the corresponding **C** samples (that is at the same spin casting speeds) are denoted as **T0**, **T1**, **T2**, and **T3**. Samples that were prepared at the same spin casting speed but had a slightly different thickness (resulting in different cavity resonance wavelengths and detunings in **C** samples) are labeled with "a," "b," or "c" (e.g., **C3a**), Table 1.

2.2. Optical Measurements. In all samples, reflectance and transmittance were measured using a vertical, custom-built optical assembly mounted to an inverted microscope (Olympus IX-71). White light from a fiber-coupled tungsten filament source (Ocean Optics LS-1) was used to illuminate samples at normal incidence from the exposed film side (through air in **B** samples or through a glass substrate in **T** samples). Reflected or transmitted light was then detected via fiber-optic cable using an Ocean Optics USB2000-FLG spectrometer. Photoluminescence (PL) spectra were measured under 532 nm continuous wave (cw) excitation from a Verdi-5 laser (Coherent, Inc.) focused by a 10× microscope objective. Optical constants and film thicknesses were obtained using a V-VASE J.A. Woolam spectroscopic ellipsometer as described in detail in the SI and pertinent parameters listed in Table S1.

The microcavities were characterized using angle-resolved reflectance on a custom-built optical assembly. White light from a fiber-coupled tungsten filament source (Ocean Optics LS-1) was passed through a linear polarizer to select either s- or p-polarizations before being focused onto the sample with a 10 cm focal length lens at angles of incidence ranging from 20 to 80° in steps of 5°. Reflected light was then collected and analyzed with an Ocean Optics USB2000-FLG spectrometer.

PL lifetime measurements were performed with 532 nm excitation from a frequency-doubled 1064 nm picosecond pulsed laser (HE-1060, Fianium, Inc.). Time-resolved PL was detected via fiber-optic cable coupled with a single-photon avalanche photodiode (SPAD, Molecular Photonic Devices) and a time-correlated single-photon counting card (TimeHarp 200, Picoquant, Inc.). PL lifetimes in thin films of each sample geometry were measured both before and after 30 min of continuous irradiation with a 532 nm cw laser to determine the effects of molecular photodegradation on PL decay dynamics.

Details of spectral analysis for the "bare" films in **B** and **T** samples and coupled films in **C** samples, as well as the polaritonic model used in extracting the exciton−photon coupling strengths from angle-resolved reflectance data from the **C** samples, are described in the SI.

2.3. Photodegradation Experiments. To induce photodegradation, samples were irradiated at normal incidence using either unpolarized white light from a tungsten halogen lamp (Dolan-Jenner Fiber Lite DC950) focused by a 50× microscope objective or circularly polarized 532 nm continuous wave excitation from a Verdi-5 laser (Coherent, Inc.) focused by a 10× microscope objective. Laser excitation for all samples was performed through the Ag layer, while white-light excitation

Table 1. Properties of Cavity Samples Used in Our Studies

spin casting speed	sample	E_0 (eV) (λ_0 (nm))[a]	Δ (meV)[b]	λ_{LP} at $\theta = 0$ (nm)[c]
2200 RPM	**C0**	2.45 (506)	126	557
1700 RPM	**C1a**	2.34 (530)	12	573
1700 RPM	**C1b**	2.33 (532)	6	574
1500 RPM	**C2a**	2.26 (550)	−71	587
1500 RPM	**C2b**	2.25 (551)	−77	588
1500 RPM	**C2c**	2.22 (559)	−107	594
1200 RPM	**C3a**	2.09 (593)	−236	627
1200 RPM	**C3b**	2.06 (602)	−267	639
1200 RPM	**C3c**	2.00 (620)	−328	680

[a]E_0 is the cavity photon energy at normal incidence ($\theta = 0$), and λ_0 is the corresponding fundamental mode resonance wavelength in cavities. [b]Detuning, defined as $E_0 - E_X$ where E_X is the energy of the 0−0 exciton in TIPS-Tc. Red detuning = negative values of Δ. [c]Wavelength of the lower polariton (LP) branch at $\theta = 0$. In **C3** samples deposited using a lower spin casting speed of 1200 RPM, a larger sample-to-sample variation was observed in film thicknesses resulting in a larger spread of LP properties and detuning as compared to thinner films in **C1** and **C2** samples.

https://doi.org/10.1021/acs.jpcc.1c06881
J. Phys. Chem. C 2021, 125, 27072−27083

came from the exposed side of the film (opposite side to laser excitation in **C** samples). The reflectance of the white light was detected at normal incidence through a vertical, custom-built optical assembly connected via fiber-optic cable to an Ocean Optics spectrometer (USB2000-FLG). The photodegradation-inducing light beam was blocked from detection with an automated beam block to periodically block excitation during reflectance measurements to prevent spectrometer saturation. Irradiation periods of 5 s were significantly longer than detection (rest) periods of 150−350 ms. The beam block was also used during recovery measurements to allow the films to recover in the dark for a set period of 10−20 min. Given the irradiation intensity dependence of photodegradation rates in all samples, all measurements on cavities were accompanied by side-by-side measurements on control **T** samples, to account for day-to-day variation in irradiation conditions. We refer to samples before the exposure to the photodegradation-inducing light (i.e., exposure time $t = 0$) as "fresh" and to those after the exposure as "irradiated."

To determine the availability of oxygen to the **T** and **C** samples—because of either permeation through the Ag film or the sides of the samples, or because of having been trapped in the films during Ag deposition—**B** samples were photobleached both in air and under vacuum in a Janis STC-500 cryostat. We refer to the samples bleached in air as **B** and the samples bleached in vacuum as **B(V)**. The procedure used for collecting data in the cryostat was the same as for films exposed to air. As a control for thermally induced reactions, the reflectance spectra of **T** samples were measured before and after a heat treatment at 60 °C in the dark, at a 10 min interval, for 40 min, and no spectral changes were noted.

2.4. Density Functional Theory (DFT). The molecular configuration of TIPS-Tc was explored using DFT. The ground-state geometry of TIPS-Tc was optimized using the B3LYP functional with the 6-311G+(2d,p) basis set, yielding also the frontier molecular orbital energies. Next, the first two allowed singlet excited-state (vertical) transition energies $E_{S0\text{-}Sn}$ along with the corresponding oscillator strengths $f_{S0\text{-}Sn}$ (for $n = 1, 2$) were calculated using time-dependent (TD) DFT methods at the same level of theory. The same calculations were repeated for the Tc molecule with the TIPS side groups interchanged for SiH_3 groups, which were also used for calculations on endoperoxides (EPOs) and photodimers discussed below.[26] A visualization of the highest occupied molecular orbital (HOMO) and lowest unoccupied molecular orbital (LUMO) for SiH_3-Tc is given in Figure S2. To explore the photodegradation pathways for TIPS-Tc, several candidate molecules were studied. When oxygen is present (**B** samples), acenes are known to form EPOs, and so the two possible EPOs were geometrically optimized and then TD DFT was used to predict the first two excited states using the same methodology as described above. Additionally, the natural transition orbitals were calculated, as described in our previous publication.[26] Tc-EPO_A is where the oxygen molecule bonds on the center ring without the side groups (see Figure S6), and Tc-EPO_B is where it bonds across the same ring as the side groups. In **T** and **C** samples, a dimer-based alternative photodegradation pathway was explored, denoted (Tc + Tc) in Table 3. As discussed in Section 3.2, in this dimer the triple bonded carbons of the side group of one TIPS-Tc molecule bond across the ring structure of the other TIPS-Tc molecule just as an oxygen molecule would for EPO formation. The same geometry optimization and excited-state calculations were performed on this molecule.

3. RESULTS

3.1. Optical Properties and Photodegradation of TIPS-Tc Films in Air. Optical properties of TIPS-Tc films used in our studies were similar to those previously reported for disordered TIPS-Tc films (Figures 1 and S2).[22] Briefly, the optical absorption spectra exhibited a pronounced vibronic progression (Figures 1 and 2) with a 0−0 exciton energy E_X of 2.32 eV, a linewidth σ_0 of 48 meV, and a vibrational energy E_V of 0.17 eV (Table 2 and SI). The molecular orbitals involved in the S_0-S_1 transition obtained using DFT methods are shown in Figures S2 and S3. The PL spectra revealed the presence of two emissive species, the S_1 excitons with a 0−0 energy of 2.30 eV and a lifetime of ∼2 ns and the correlated pair of triplet states (TT), formed in the process of singlet fission ($S_0 + S_1 \rightarrow TT \rightarrow T_1 +$

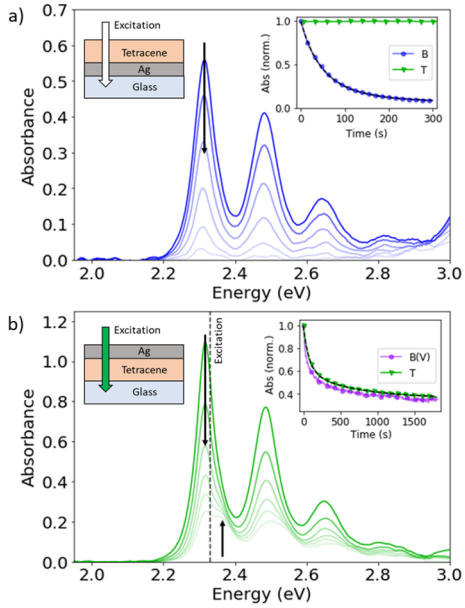

Figure 2. (a) Absorbance of a **B** sample in air under continuous exposure to white light at 0.19 W/cm^2. Left inset: schematics of a **B** sample and illumination geometry. Right inset: time evolution of the total integrated S_0-S_1 absorbance, normalized at its value at $t = 0$, of a **B** sample in air and in a **T** sample under the same white-light exposure via the film side in both samples. A bi-exponential fit to the **B** data in the inset is shown as a dashed line. (b) Absorbance of a **T** sample over time under continuous exposure to 532 nm cw light at 27 W/cm^2. Left inset: Schematics of a **T** sample and illumination geometry. Right inset: time evolution of the total integrated S_0-S_1 absorbance, normalized at its value at $t = 0$, of **T** and **B(V)** samples under the same 532 nm cw exposure. For direct comparison between **T** and **B(V)** samples, both samples were irradiated through the Ag layer.

Table 2. Optical Properties of TIPS-Tc Monomers and Alkyne Dimers

molecule	E_X (eV)[a]	E_V (eV)[a]	S[a]	σ (eV)[a]	$\Delta\sigma$[a]	$E_{S0\text{-}S1}$ (eV)[b]
monomer	2.32	0.17	0.96	0.048	0.54	2.09
dimer	2.37	0.17	0.90	0.065	0.30	2.19

[a]E_X, E_V, S, σ, and $\Delta\sigma$ are the 0−0 exciton energy, vibrational energy, Huang−Rhys factor, Lorentzian width, and width expansion, respectively, obtained from fits to data of Figure 3a for the TIPS-Tc monomer and the alkyne dimer to eq (S2).[27,28] [b]$E_{S0\text{-}S1}$ is the energy of the S_0-S_1 transition calculated using TD DFT as described in Section 2.4.

https://doi.org/10.1021/acs.jpcc.1c06881
J. Phys. Chem. C 2021, 125, 27072−27083

T_1),[22] with the energy peaked at ∼1.92 eV and a lifetime of ∼13 ns (Figures S4 and S5). The properties of TT states of varying multiplicity (e.g., ^{1}(TT) and ^{5}(TT)) in TIPS-Tc films, depending on film morphology, have been previously reported,[22,24] and a 180% yield of free triplet states T_1, originating from thermally activated TT state dissociation, was observed in disordered TIPS-Tc films such as ours. Here, we will focus on the TT state with a singlet character, ^{1}(TT), which will be for simplicity referred to as TT, unless stated otherwise. Briefly, the TT state in TIPS-Tc films forms on multiple time scales (from <100 fs to tens of ps),[22,24] after which it can emit PL at time scales of tens of ns, convert to free triplet states (T_1), or geminately recombine back to S_1 contributing to the delayed fluorescence from the S_1 state. The relevance of these properties to the photochemical processes described in the present study will be discussed in Sec. 4.

Next, we explored how the optical properties of the TIPS-Tc films described above changed upon continuous white-light exposure, depending on the sample configuration. Figure 2a shows the time evolution of the absorption spectra in a **B** sample in which the TIPS-Tc film was exposed to air, under continuous 190 mW/cm^2 white-light irradiation. Fast degradation was observed, with the S_0-S_1 absorption of TIPS-Tc molecules decreasing by an order of magnitude after only ∼3 min of exposure, with no new spectral features detected in the visible wavelength range. No degradation was observed under the same irradiation conditions in a **T** sample (inset of Figure 2a), where the TIPS-Tc film is encapsulated by the top Ag layer, which suggests that the fast photodegradation in the TIPS-Tc film exposed to air predominantly follows an oxygen-dependent pathway. The integrated S_0-S_1 absorption (inset of Figure 2a), normalized by its value for a fresh sample (i.e., at the exposure time $t = 0$), was well described by a bi-exponential function of the form $a_{1a} \exp(-k_{1a} t) + a_{2a} \exp(-k_{2a} t) + a_{0a}$, where k_{1a} and k_{2a} are the degradation rates in air, a_{1a} and a_{2a} are corresponding weights, a_{0a} is a residual absorption by TIPS-Tc molecules unaffected by these degradation processes, and $a_{0a} + a_{1a} + a_{2a} = 1$. The rates yielded values of $k_{1a} = 0.0295 \pm 0.0005$ s^{-1} and $k_{2a} = 0.0116 \pm 0.0002$ s^{-1} for these exposure conditions, contributing similarly ($a_{1a}/a_{2a} = 0.84 \pm 0.05$) to the decay dynamics, with only a small (∼7%) residual population ($a_{0a} = 0.070 \pm 0.005$) of TIPS-Tc molecules not subjected to the degradation under these conditions. Examination of multiple **B** samples measured under various irradiation conditions revealed irradiation intensity-dependent rates but intensity-independent residual population ranging between 4 and 7% depending on the sample morphology. We attribute the observed processes occurring in air to the photo-oxidation with the formation of EPOs, which is a known photodegradation mechanism in acenes exposed to air.[25] The two possible Tc-EPO configurations (where the oxygen molecule bonds across the center ring without TIPS groups, Tc-EPO_A, and across the same ring as the TIPS side groups, Tc-EPO_B), which have been previously identified at a 2:1 ratio in photo-oxygenated TIPS-Tc solutions,[25] were examined using DFT (Table 3 and Figure S6). Because of the reduced conjugation as compared to TIPS-Tc, both EPO derivatives have optical absorption in the UV region, with the DFT-predicted S_0-S_1 transitions at 3.38 and 3.80 eV for Tc-EPO_A and Tc-EPO_B, respectively, which is consistent with the lack of new spectral features in the visible region in our experiments of Figure 2a.

3.2. Photodegradation of TIPS-Tc Films in the Absence of Oxygen. Here, we examined the photodegradation of TIPS-Tc films when the film was not exposed to oxygen, in particular in **B** samples under vacuum (denoted **B(V)**) and **T** samples. For this, we used a higher-intensity irradiation (7−70 W/cm^2 with a 532 nm cw laser) as compared to that used in experiments in **B** samples in air discussed above, to induce photodegradation on time scales closer to those of Figure 2a. Evolution of the optical absorption spectra under a continuous exposure of a **T** sample to the 532 nm cw laser light is shown in Figure 2b. Similar results were obtained for the **B(V)** samples, as illustrated in the inset of Figure 2b which shows time dependence of the integrated S_0-S_1 absorption of the **T** and **B(V)** samples, normalized by its values in the corresponding fresh samples (i.e., at the exposure time $t = 0$). The similarity of the **B(V)** and **T** traces indicates that the degradation in these samples proceeds via similar, oxygen-independent mechanisms. Interestingly, in contrast to a monotonic reduction in the absorption across the visible wavelengths for TIPS-Tc films exposed to air (**B** sample in Figure 2a), the absorption in **T** and **B(V)** samples developed a new spectral feature, with the main peak blue-shifted by only ∼0.05 eV from the 0−0 absorption line of TIPS-Tc, which grew in time under a continuous 532 nm light exposure (Figures 2b, 3a and S8). This new feature is apparent from fits of the absorption spectra (as described in detail in the SI),[27,28] which evolve from one vibronic progression for the TIPS-Tc monomer in the fresh sample (at time $t = 0$) to two vibronic progressions (TIPS-Tc monomer and a new species) at later times (Figures 3a and S8), with the fit parameters listed in Table 2.

A prominent oxygen-independent photodegradation pathway in acenes is a photodimerization, which has been extensively studied,[29−33] and dimer formation pathways were investigated.[34−36] However, most of the studies focused on the "butterfly" dimers, where the conjugation is broken for both monomers forming a dimer. Such dimers absorb in the UV and do not contribute to the absorption in the visible wavelength region.[29] While it is likely that "butterfly" dimers form in TIPS-Tc, as discussed below, these are not the photoproducts with absorption spectra revealed by experiments of Figure 3a. Instead, we hypothesize that the new species formed in the **B(V)** and **T** samples under light exposure are alkyne dimers with the molecular structure shown in the inset of Figure 3a (bottom), qualitatively similar to those observed in other functionalized acene derivatives upon degradation.[37,38] This assignment is in agreement with DFT calculations of optical

Table 3. Results from *Ab Initio* Calculations for Each Molecular System Including Results for TIPS-Tc, SiH_3-Tc, Tc-EPO_A, Tc-EPO_B, and (Tc + Tc)[a]

molecule	E_{HOMO}	E_{LUMO}	$E_{S_0-S_1}$ ($f_{S_0-S_1}$)	$E_{S_0-S_2}$ ($f_{S_0-S_2}$)
TIPS-Tc	−5.149 eV	−2.788 eV	2.095 eV (0.2314)	3.126 eV (0.0526)
SiH_3-Tc	−5.374 eV	−3.027 eV	2.087 eV (0.1663)	3.117 eV (0.0486)
Tc-EPO_A	−6.265 eV	−2.516 eV	3.381 eV (0.1739)	3.526 eV (0.2532)
Tc-EPO_B	−6.347 eV	−1.675 eV	3.798 eV (0.0049)	4.085 eV (0.0228)
(Tc + Tc)	−5.253 eV	−2.756 eV	2.188 eV (0.1590)	2.484 eV (0.0021)

[a]The frontier orbital energies (E_{HOMO} and E_{LUMO}) were calculated using DFT (B3LYP/6−311 + G(2d,p)), while the first and second allowed singlet transition energy (vertical) and oscillator strength ($E_{S0\text{-}Sn}$ and $f_{S0\text{-}Sn}$, respectively, where $n = 1, 2$) were calculated using TD DFT methods at the same level of theory.

https://doi.org/10.1021/acs.jpcc.1c06881
J. Phys. Chem. C 2021, 125, 27072−27083

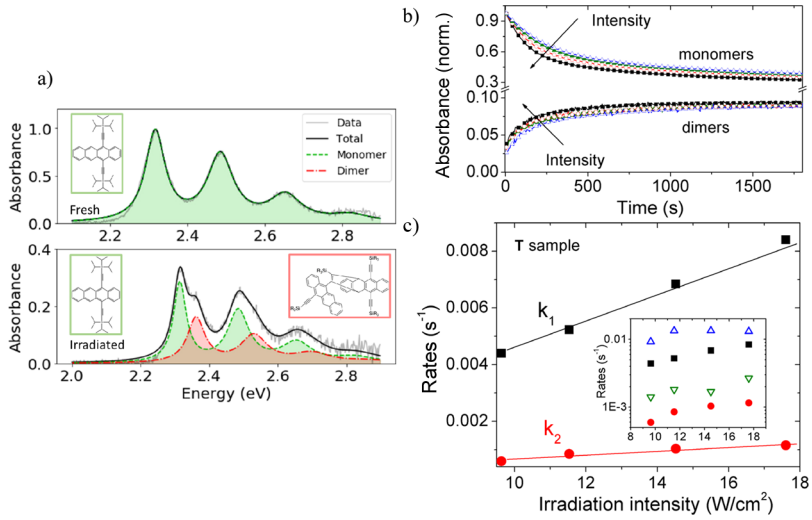

Figure 3. (a) Absorbance of a **T** sample before (top) and after (bottom) 30 min of continuous irradiation with a 532 nm cw laser light at 18 W/cm^2. The green (red) area under absorption spectra corresponds to the absorbance of TIPS-Tc molecules (alkyne dimers), shown in the left (right) inset. The spectral fits and deconvolution into two vibronic progressions were performed using a model of eq (S2) as described in the SI; the fit parameters are listed in Table 2. (b) Dynamics of the TIPS-Tc monomer concentration decay and alkyne dimer formation obtained by integration of the corresponding absorption spectra (green and red areas in a), respectively, at various irradiation light intensities in the 9−18 W/cm^2 range (lines). Both monomer and dimer integrated absorption spectra were normalized by the total integrated absorption at $t = 0$. Bi-exponential fits to each trace, both for the monomer decay and for the alkyne dimer rise, are shown as lines with symbols. Break in the y-axis is introduced for clarity. (c) Rate constants k_1 and k_2 obtained from bi-exponential fits to the monomer decay as functions of irradiation intensity (I). Linear fits ($k_{1,2} - I$) are shown with lines. The inset shows comparison of the k_1 and k_2 rates for the monomer decay (closed symbols) and k_{1d} and k_{2d} rates obtained from the bi-exponential rise of the alkyne dimer population (open symbols) at various irradiation intensities I.

properties of such dimers (Tables 2 and 3 and Figure 4), which confirm that the energy of the S_0-S_1 transition for the proposed alkyne dimer is only slightly higher than that of the parent TIPS-Tc molecule. This is expected because the conjugation of one of the monomers in the dimer is mostly preserved (Figures 4 and S9), and it is consistent with the optical absorption data of Figure 3a.

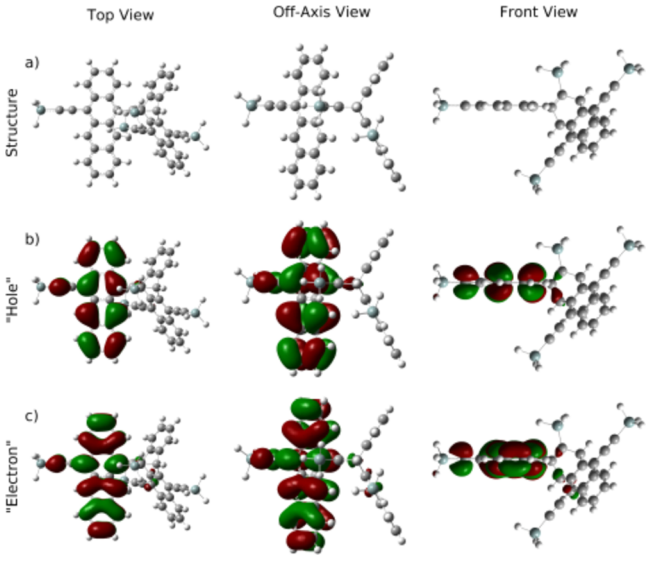

Figure 4. Structure (a) and natural transition orbitals (b and c) for the S_0-S_1 transition for the alkyne dimer (Tc + Tc in Table 3). (b) Initial state for the transition (analogous to the "hole" wavefunction) and (c) final state for the transition (analogous to the "electron" wavefunction). Note that "hole" and "electron" wavefunctions are primarily concentrated on the undistorted Tc backbone and that they are qualitatively similar to the "hole" and "electron" states of SiH_3-Tc (see Figure S3), suggesting that this dimer's excited state has a similar character to the S_0-S_1 state for a monomer. The calculations were performed using TD DFT methods (B3LYP/6−311 + G(2d,p)).

The dynamics of the monomer decay and alkyne dimer formation obtained by integrating the absorption spectra of the monomer (green area in Figure 3a) and alkyne dimer (red area in Figure 3a) upon irradiation are shown in Figure 3b, at various 532 nm irradiation light intensities. At all intensities studied, these dynamics were well described by a bi-exponential function ($a_0 + a_1 \exp(-k_1 t) + a_2 \exp(-k_2 t)$ and $a_{0d} - a_{1d} \exp.(-k_{1d} t) - a_{2d} \exp(-k_{2d} t)$ for the monomer decay and alkyne dimer formation, respectively), with a_i and a_{id} (i = 0,1,2) coefficients independent of the irradiation intensity(I), whereas the rates scale linearly with I (Figure 3c).

The presence of fast and slow components in the photodimerization dynamics has been previously observed[32,39] and attributed to a fast dimerization of the molecules with a favorable orientation (fast initial decay) which then slows down as the exciton search time for a pair of molecules with favorable orientation increases (slower decay, which then levels off at a nonzero value of a_0). It is possible that similar considerations are applicable to our case as well, as we observed shortening of the PL lifetimes after the prolonged irradiation (Figure S10a), which indicates that the presence of photodimers induces PL quenching which could lead to kinetics heterogeneity.[32] However, other scenarios, such as formation of multiple photoproducts[37] (contributing to the heterogeneity in the monomer decay), as discussed below, and existence of two independent pathways of alkyne dimer formation that proceed via different intermediates (contributing to the bi-exponential dynamics of the alkyne dimer formation) cannot be ruled out.

Comparison of the reaction quantum yields ϕ (defined using $k = I_{ph,abs}\phi$, where $I_{ph,abs}$ is the absorbed irradiation photon flux and k is the rate extracted from the fits of the monomer decay

https://doi.org/10.1021/acs.jpcc.1c06881
J. Phys. Chem. C 2021, 125, 27072−27083

dynamics) for the faster degradation processes in **B** and **T** samples described by k_{1a} and k_1 rates, respectively, indicates that the oxygen-independent degradation process in **T** samples is a factor of ~650 less efficient than the oxygen-mediated degradation in air in **B**. This explains why the alkyne dimer formation was not readily observed in TIPS-Tc films exposed to air and the alkyne dimer spectral features were not detected in the **B** data of Figure 2a. Interestingly, in the **T** samples, the residual monomer absorption a_0 was in the 0.16−0.3 range (Figures 3b and S8), depending on the sample morphology, indicating that 16−30% of the TIPS-Tc molecules in these films are in configurations that are not conducive to oxygen-independent degradation mechanisms. These percentages are considerably higher than only 4−7% of TIPS-Tc molecules that remained unaffected by the EPO formation when the film was exposed to air. Furthermore, the contribution of the absorbance from the alkyne dimers after prolonged irradiation (given by a_{0d}) constitutes only about 10−17% of the initial total absorbance (Figures 3b and S8). Because the oscillator strength of the alkyne dimer is comparable to that of the monomer (Table 3), but only one of the two moieties in the alkyne dimer absorbs in the visible wavelength range, this translates into about 20−34% of the initially present TIPS-Tc molecules that convert into the alkyne dimer of Figure 3a after a prolonged light exposure. Given that about 70−84% of the monomers convert to photoproducts (Figures 3b and S8), this suggests that up to 50% of monomers convert into other products, such as "butterfly" dimers widely discussed in the literature.[29−33] This conversion must be occurring slower than the alkyne dimer formation which explains about a factor of ~2−3 slower overall dynamics of the monomer decay as compared to that of alkyne dimer formation (inset of Figure 3c and Figure S8b).

3.3. Photodegradation of TIPS-Tc Strongly Coupled to Microcavities. When placed in microcavities, the TIPS-Tc films exhibited signatures of strong exciton−photon coupling (Figures 5 and S11−13). Figure 5a shows angle-resolved reflectance spectra obtained from a cavity resonant with the 0−0 transition in TIPS-Tc (**C1b**, Table 1). All three exciton transitions (0−0, 0−1, and 0−2) within the S_0-S_1 absorption band of the TIPS-Tc film coupled to the cavity photon creating the LP, two middle polariton (MP1 and MP2), and the upper polariton (UP) branches (Figures 5b and S12), with the coupling strengths ($2V_{0i}$, i = 0,1,2), extracted from fits to the coupled oscillator model (see the SI), scaling as expected with the oscillator strength[40] (Figure S13) and exhibiting values of up to ~290 meV (Table S3).[18] Because of the similarity between the **T** and **C** samples in terms of oxygen availability, we expect that in the cavities (**C** samples) the photodegradation processes are similar to those discussed above for the **T** samples, and therefore, we examined the photodimerization of TIPS-Tc molecules in cavities side by side with those in the **T** samples under the same irradiation conditions.

Figure 6a shows a photodimerization-induced change in the reflectance spectra obtained from a resonant cavity **C1b** under continuous 532 nm irradiation, with the time evolution of energies (positions of the reflectance minima) for LP, MP1, and MP2 polariton branches summarized in the inset of Figure 6a). The observed energy shifts are due to a time-dependent reduction in the exciton-coupling strengths ($2V_{0i}$, Table S3) caused by a decreasing concentration (N) of the surviving TIPS-Tc molecules coupled to the cavity, as expected from the $2V_{0i} \sim N^{1/2}$ relationship.[12,14,40] The decay in the TIPS-Tc concentration (N) obtained from the time-dependent coupling

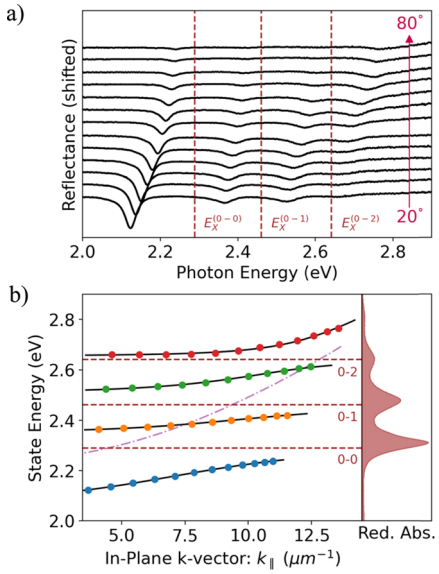

Figure 5. (a) Angle-dependent reflectance spectra for TIPS-Tc in a resonant cavity **C1b**. Vertical dashed lines label exciton resonances in TIPS-Tc corresponding to 0−0, 0−1, and 0−2 transitions. (b) Dispersion characteristics obtained from reflectance dip positions in the data in (a) (dots) fit with the coupled oscillators model (lines) yielding coupling strengths $2V_{00}$ = 258 meV, $2V_{01}$ = 220 meV, and $2V_{02}$ = 138 meV. LP (blue dots), middle polariton 1 (MP1) (orange dots), middle polariton 2 (MP2) (green dots), and UP (red dots) branches are shown. The dash-dotted line corresponds to the dispersion of the cavity photon, and horizontal dashed lines show the energies of the excitons in "bare" (uncoupled to the cavity) TIPS-Tc films for which the absorption spectrum is included on the right.

strength $2V_{00}$ as $N \sim (2V_{00})^2$ for the **C1b** normalized at its value at t = 0 is shown in Figure 6b. For comparison, the integrated S_0-S_1 absorption data obtained in the **T1b** control sample under the same irradiation conditions (i.e., through the Ag/TIPS-Tc film interface in both cases) are also included in the figure.

The N(t) dynamics in **C1b** of Figure 6b were fit by a bi-exponential function ($a_{0c} + a_{1c}\exp.(-k_{1c}t) + a_{2c}\exp.(-k_{2c}t)$); fit parameters for **C1b** and the **T1b** control sample are summarized in Table S2b. In **C1b**, the rate k_{1c} = 0.0344 ± 0.0008 s^{-1} was a factor of 1.97 ± 0.07 higher than the corresponding rate k_1 = 0.0175 ± 0.0002 s^{-1} in the **T1b** control sample. The residual fraction of TIPS-Tc molecules unaffected by photodimerization described by a_{0c} was 0.195 ± 0.001 in **C1b**, which is lower than a_0 = 0.303 ± 0.001 in **T1b**. This suggests that (i) the population of TIPS-Tc molecules that efficiently couples to the cavity has a preferential intermolecular orientation and relevant excited-state dynamics that is more prone to photodimerization as compared to the overall population probed in the **T** samples and/or (ii) polariton states facilitate the chemical reaction in molecules which otherwise would not be susceptible to these photochemical processes, as discussed in Sec. 4.2.

To understand the underlying mechanisms behind the differences in oxygen-independent photodegradation dynamics in the **C1** and **T1** samples in Figure 6b, and recalling the linear light intensity dependence of reaction rates on light intensity in Figure 3c, it is necessary to account for the differences in the absorbed photon flux in the organic layer in these two sample configurations. A unified approach to this calculation, which would be important for the emerging field of polariton-modified photochemistry, has not yet been developed, and the current

https://doi.org/10.1021/acs.jpcc.1c06881
J. Phys. Chem. C 2021, 125, 27072−27083

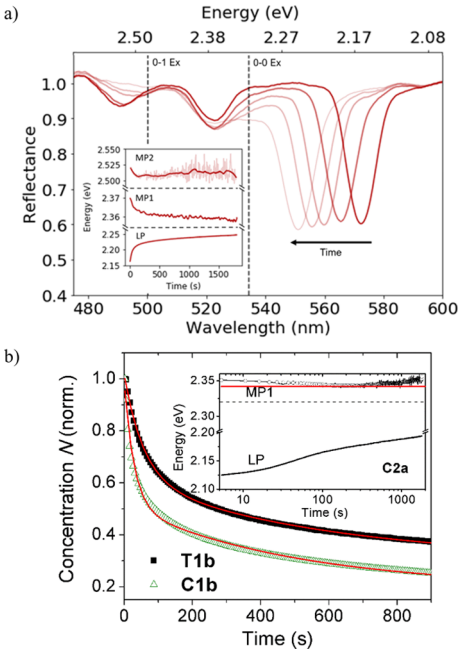

Figure 6. (a) Time evolution of reflectance spectra for TIPS-Tc polaritons in a resonant cavity **C1b** upon continuous 532 nm cw light irradiation at 37 W/cm^2. Vertical lines show the wavelengths (energies) of excitons that couple to the cavity. (b) Concentration (N) of TIPS-Tc molecules in the **C1b** and **T1b** samples as a function of time under continuous irradiation with a 532 nm laser light normalized at the corresponding values at t = 0. Bi-exponential fits are also shown (red lines). The inset shows time evolution of energies of the LP and MP1 branches in the **C2a** cavity. The dashed gray line corresponds to the 0−0 exciton energy; the red line highlights a nonmonotonic MP1 branch evolution because of the alkyne dimer coupling to the cavity.

approaches vary across the literature.[12−14,24] Similar to the approach in ref 14, we used the transfer matrix method to obtain the distribution of electromagnetic field across the film in the **C** and **T** samples (Figure S14) at 532 nm illumination, which accounts for phase changes occurring in semitransparent Ag mirrors and interference effects resulting from internal reflections (which are important in our 95−140 nm thick films). Because this wavelength is close to the **C1b** resonance (Table 1), the light intensity in the active TIPS-Tc layer in **C1b** is enhanced by a factor of ∼10.3 (obtained from integrating the $|E|^2$ profiles in Figure S14 across the film, Table S4) as compared to that in the **T1b**. (Such enhancement is a feature of cavity structures that has been utilized in cavity-enhanced absorption spectroscopy, as well as in improving light trapping in solar cells and enhancing LED emission.[41,42] This enhancement is expected to vary significantly with the detuning between the wavelength of cavity resonance and the illumination wavelength, which we probe by varying film thicknesses between samples. In particular, as the detuning increases, the enhancement drops precipitously, as seen from Figure S14 and Table S4. The other factor we explicitly took into account is the presence of strong exciton−photon coupling, which redistributes the oscillator strength, causing the total absorbed fraction of the incident 532 nm light in the **C** samples (excited in the vicinity of the MP1 branch, Figure 6a) to be considerably lower than that in the **T** samples (in which the 532 nm light is almost resonant with a strong 0−0 line of TIPS-Tc molecules, Figures 1 and S1). Strong $|E|^2$ enhancement, scaled by a low overall absorbed fraction of light, in **C** samples as compared to **T** samples, results in an absorbed photon flux ratio of 0.47 in **C1b** as compared to **T1b** (Table S4). As a result, at the same incident intensity of the 532 nm irradiation, the k_{1c} rate in **C1b** cavities would be expected to be 0.47 of the k_1 rate in the **T1b** (Table S4)− thus, slower. This is in contrast to a factor of 1.97 faster rate observed in **C1b** as compared to **T1b** samples (Figure 6b), which translates into a factor of ∼1.97/0.47 = 4.2 higher quantum yield of the dimerization in the **C1b** cavity. Several considerations could be behind this observation, which are discussed in Sec. 4.2.

Next, we explored time evolution of polariton energies caused by photodegradation, depending on the energy offset between the cavity photon and the 0−0 exciton (cavity detuning Δ), which enables varying the relative contributions of the photonic and excitonic components in the polariton states (e.g., the LP states probed at normal incidence in red-detuned cavities **C2** and **C3** have a higher photonic component as compared to those in resonant cavities **C1**). The inset of Figure 6b illustrates changes in the LP and MP1 energies upon continuous 532 nm irradiation in the **C2a** cavity; data for other cavities are shown in Figure 7a. Similar to the dynamics in the **C1b** resonant cavity (inset of Figure 6a), in all cavities the LP branch experienced the most pronounced shift, of all branches. In several cavities, including **C2a**, a nonmonotonic behavior in the peak shift dynamics was observed at longer irradiation times (>300 s) (inset of Figure 6b). We attribute this behavior, with an onset corresponding to the times when a sizable population of photoproducts had been generated, to the coupling of the alkyne dimer of Figure 3a to the cavity which shifts the overall polariton energies. For simplicity, we focus only on the dynamics at shorter time scales (t < 300 s, Figure 7b) and on the LP branch.

To aid the comparison with the control **T** samples, the LP dynamics were fit by a bi-exponential function (Figure 7b and Table S2c). The ratios of the faster rate k_{1LP} in cavities with various detunings and the faster rate k_1 in corresponding control **T** samples (which accounts for a slight effect of film thickness, independent of the strong coupling effects, on the rates, Figure S15 and Table S2(a)), relative to that obtained in the resonant cavity **C1b**, are shown in Figure 7c. Only a slight change in the LP dynamics was observed upon detuning in our detuning range, with the k_{1LP}/k_1 ratio tending toward lower values at larger red-detunings |Δ|. Accounting for the differences in the absorbed photon flux of the photodimerization-inducing 532 nm light ($I_{ph,abs}$) (Table S4) among various cavities calculated as discussed above for the **C1b** cavity, the photodimerization quantum yield EF (defined as EF = ϕ_C/ϕ_T, where ϕ_C (ϕ_T) are quantum yields for the **C** (**T**) samples obtained from k_{1LP} (k_1) rates assuming $k = I_{ph,abs}\,\phi$) normalized by that for the **C1b** cavity (inset of Figure 7c) and averaged over two or three cavities in each detuning range (**C1**-**C3**), tends toward slightly higher values upon red detuning, thus potentially exhibiting an even stronger speed-up of the TIPS-Tc photodimerization than the factor of 4.2 observed in the resonant cavity **C1b**. However, systematic studies relating the time evolution of the LP branch to that of the coupling strengths $2V_{0i}$, depending on the cavity detuning, are needed to obtain a quantitative relationship between the dynamics of the population of the strongly coupled molecules N and of the LP branch energy shifts in detuned cavities. Nevertheless, the observed weak detuning dependence of the photodimerization-induced LP shift dynamics is interesting, and it mirrors previous work on TIPS-Tc cavities[24] where a weak cavity detuning dependence of polariton-mediated delayed PL was observed in a relatively large detuning range (up to −545 meV), as discussed in Section 4.2.

https://doi.org/10.1021/acs.jpcc.1c06881
J. Phys. Chem. C 2021, 125, 27072−27083

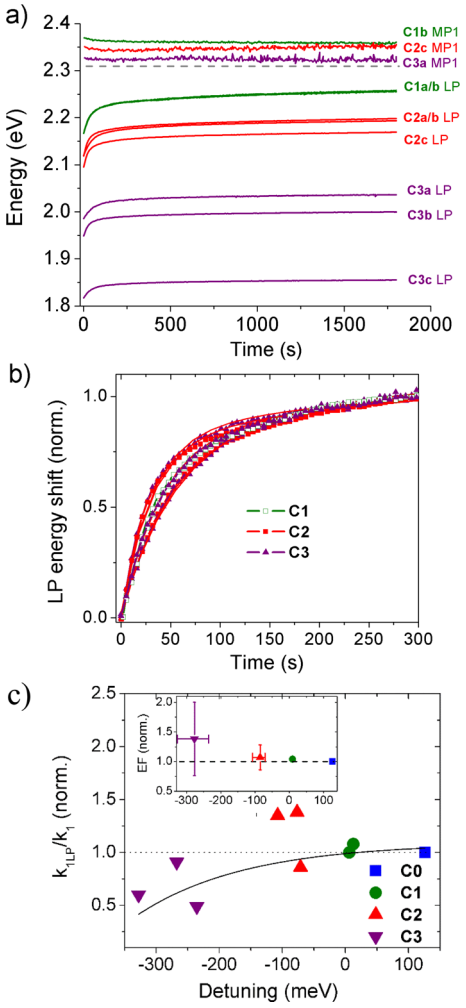

Figure 7. (a) Time evolution of energies of the LP and MP1 branches in **C1a-b, C2a-c,** and **C3a-c** cavities upon continuous 532 nm irradiation caused by photodimerization (lines with symbols). (b) Time evolution of the LP energy illustrated as $(E_{LP}(t)\text{-}E_{LP}(0))/(E_{LP}(300\ s) - E_{LP}(0))$ in all **C** samples studied. The bi-exponential fits $(a_{0LP} - a_{1LP} \exp(-k_{1LP} t) - a_{2LP} \exp(-k_{2LP} t))$ to the data are also included (red dashed lines). The fit parameters are summarized in Table S2(c). No systematic dependence of the LP dynamics on the cavity detuning is observed. (c) Ratio of the rates k_{1LP} and k_1 obtained from bi-exponential fits to the LP branch energy shift in **C** samples and monomer decay dynamics in the corresponding control **T** samples, depending on cavity detuning. The data are normalized by the value obtained for the resonant cavity **C1b**. The line is the guide for the eye. The inset shows the enhancement factor (EF) defined as the ratio of reaction quantum yields in a cavity **C** and a corresponding control sample **T**, normalized by that for the resonant cavity **C1b**, for **C0**−**C3** samples. In the case of **C1**−**C3**, the data were averaged over **C1a-b**, **C2a-c**, and **C3a-c** samples (Table 1 and S4). Y-error bars reflect cavity-to-cavity variation and X-error bars represent the range of cavity detuning for that group of cavities.

4. DISCUSSION

Here, we discuss possible mechanisms behind our observations described in Section 3. Depending on whether the TIPS-Tc film is exposed to oxygen or not, the dominant photodegradation mechanism changes from the EPO formation in **B** samples to photodimerization in **T** or **C** samples. Furthermore, there is evidence that at least two types of photodimers form, one of which is the alkyne dimer (Figure 4) and the other one is most likely a "butterfly" dimer.[43] Although establishment of the exact pathway and the excited states responsible for EPO formation and photodimerization in our disordered TIPS-Tc films requires further studies, we comment on how our results fit into what is known about relevant photochemical reaction pathways from the literature.

4.1. EPO Formation. Because of the considerable importance of acene derivatives in organic electronics, acene−oxygen interactions have been extensively studied.[33] The two pathways for these photochemical interactions have been identified to occur via electron transfer (Type I) or energy transfer (Type II) to ground-state oxygen. The Type I process proceeds from the S_1 state of acene and results in the formation of an acene cation and superoxide (O^{2-}). The Type II process typically proceeds via the intersystem crossing (ISC) to form a T_1 state on the acene molecule followed by the energy transfer to the ground-state oxygen molecule ($^3O_2$), which yields singlet oxygen ($^1O_2$). Both O^{2-} and $^1O_2$ are reactive species that could attack the acene molecule leading to the EPO formation, which is the main product toward decomposition.[25]

It has been documented that in Tc derivatives, the EPO formation predominantly proceeds via the Type II process which is made efficient by the T_1 energy of Tc (1.2−1.3 eV in TIPS-Tc)[22] being higher than the singlet−triplet gap for oxygen (0.98 eV).[25] How the presence of entangled triplet pairs (TT states), which are prominent in TIPS-Tc films, affects these general considerations above has not been discussed in the literature. However, it would be reasonable to assume that even if the TT state itself does not generate the reactive oxygen species, the singlet fission and the associated increased yield of T_1 states formed via dissociation of TT as compared to those generated from S_1 via ISC would promote EPO formation via the Type II mechanism. It has been previously reported[22] that the TT state dissociation into free triplet states T_1 in disordered TIPS-Tc films is fast and efficient, and so we would expect efficient singlet oxygen generation in the vicinity of the molecular pair that had formed the TT state. "Vicinity" is defined as being well within the diffusion length for the singlet oxygen of $L = \sqrt{(6D\tau_{O2})} \approx 2.5$ nm (where D is the diffusion coefficient taken to be 10^{-9} cm^2/s[44] and τ_{O2} is the singlet oxygen lifetime τ_{O2}, assumed to be 10 μs.[45]) This makes the molecules in configurations conducive to forming TT states in these disordered films statistically more vulnerable to the oxygen attack as compared to the overall population.

Figure 8a illustrates this point by showing how the PL spectrum in **B** samples evolves under continuous exposure to the 532 nm cw irradiation. In fresh samples, the emission from TT states heavily dominates the overall spectrum. After only a few seconds of irradiation, the TT emission is considerably reduced, whereas the S_1 emission is increased, which could be realized if one of the TT state-forming molecules converts to the Tc-EPO (Section 3.1), whereas the other one remains intact and emits from the S_1 state. This conversion is followed by the degradation of the remaining molecules (and the S_1 emission decay) until only a few percent of the original TIPS-Tc monomers survive on the >100 s time scales. In agreement with previous photo-oxidation studies in functionalized acenes,[25] the Tc-EPO formation was partially reversible, as manifested in a partial recovery of PL after the sample was kept in the dark (Figure S7a). However, the only recovered PL signal was that from the S_1 state (Figure S7a). This could indicate that both molecules in the original TT configuration have degraded and that the recovery of both molecules, which is necessary to reform the TT state in **B** samples, is statistically improbable.

https://doi.org/10.1021/acs.jpcc.1c06881
J. Phys. Chem. C 2021, 125, 27072−27083

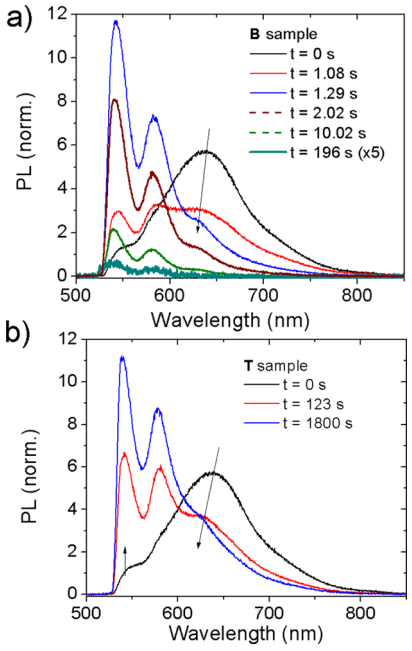

Figure 8. Time evolution of PL spectra under continuous 532 nm cw irradiation in (a) **B** sample and (b) **T** sample. In (a), the signal at $t = 196$ s was multiplied by a factor of 5 for better visibility. In both samples, the decaying contribution of the TT states with time is indicated with the down-pointing arrow. In the **B** sample, the S_1 emission first increases, reaching a maximum at between 1 and 2 s after irradiation, and then decays at times longer than 2 s. In the **T** sample, a fast rise of the S_1 emission is observed up to ~100 s followed by a slow rise and leveling off at >1500 s, with no decay during the time span of our experiments which was 3600 s.

4.2. Photodimerization. Similar to photooxygenation, the photodimerization in acenes has been extensively studied.[33] In Tc derivatives, the "butterfly" dimerization is known to proceed from a singlet (S_1) state, formed both directly and via triplet−triplet annihilation.[34,43] The alkyne dimerization in Tc derivatives has not yet been studied; however, as informed by alkyne dimerization of other functionalized acene derivatives (such as functionalized hexacene[37]), if arising from the triplet state, this reaction most likely proceeds via a stepwise mechanism, with a considerably lower driving force as compared to "butterfly" dimerization, and relying on long lifetimes of triplet states T_1. For both dimerization reactions to proceed, particular intermolecular orientations in the film are required. Alkyne dimerization imposes stricter geometrical constraints on the suitable molecular alignment as compared to "butterfly" dimerization which can tolerate slight offsets and torsions in the molecules forming the dimer.

How the TT state itself participates in these two dimerization reactions in TIPS-Tc has not yet been reported. However, even without its direct involvement in these reactions, there are two indirect implications of its presence: its efficient dissociation into free triplet states T_1 (with a 180% yield)[22] and possible geminate recombination with regeneration of the S_1 state (a process responsible for delayed PL emission from the S_1 state). These two processes would promote alkyne dimerization and "butterfly" dimerization, respectively, of the molecules participating in the TT formation and their immediate surroundings, provided the suitable intermolecular orientation requirements are met. The requirements should be easier to satisfy in disordered films such as ours as compared to crystalline.

The PL spectral evolution under continuous 532 nm irradiation of **T** samples provides an insight into the photodimerization dynamics. Similar to **B** samples, the emission from TT states in **T** samples decreases, whereas that from S_1 states increases, which would be consistent with one of the molecules originally forming the TT state participating in the photodimerization (thus TT emission decreases), whereas the other one emitting from the S_1 state (thus S_1 emission increases). In contrast to **B** samples, this process occurs in **T** samples on considerably longer time scales, and even after 30 min of continuous irradiation, there is a nonzero contribution of TT states to the overall PL emission (Figure S5b). Additionally, the S_1 emission does not appreciably decay on the time scales of our experiments (Figure 8b), which could be an indication that the surviving molecules are in orientations that are not conducive to photodimerization. It is also possible that alkyne dimers, in which one of the molecules largely preserves its molecular core (Figure 4), would emit upon 532 nm excitation. While no new PL features were observed in the PL spectra upon continuous irradiation, based on the shift in the absorption spectra of the monomer and the alkyne dimer (Figure 3b) and assuming that the Stokes shift for the alkyne dimer would be similar to that of the monomer, the two species could form a Forster resonance energy transfer pair, where the donor (dimer) absorbs light and the acceptor (monomer) emits light, thus contributing to the S_1 emission in Figure 8b at longer irradiation times.

We also note that the fast component of the decay dynamics of TT states upon continuous irradiation (probed via time evolution of PL spectra) was faster than the k_1 rates obtained from the absorption-based monomer decay dynamics under the same irradiation conditions (Figure S5). Thus, the molecules in the configurations favorable for the TT state formation and their immediate surroundings in the **T** samples degrade faster than the overall monomer population, a similar observation to that in the **B** samples in air discussed above. Additionally, the rates of the TT decay dynamics are close to those in the alkyne dimer rise dynamics, which may indicate that this state, (although most likely indirectly, by promoting free triplet T_1 generation), plays an important role in alkyne dimerization. This is consistent with the alkyne dimerization proceeding via a stepwise mechanism relying on the formation of T_1 states,[46] with an added intermolecular orientation constraint necessary for dimerization. Given that the degraded emission from the TT state in **T** or **B(V)** samples was partially reversible after the sample was kept in the dark (Figure S7b and c), which is the only reversible behavior observed in these samples, we hypothesize that one or both molecules forming the TT state are susceptible to the "butterfly" dimerization as well, which we expect to be more reversible than the alkyne dimerization.

Next, we discuss possible mechanisms for the polariton involvement in photodimerization in **C** samples, which manifested through rate enhancement (k_{1c}) and the higher fraction of photoconverted molecules ($1-a_{0c}$), as compared to control **T** samples (Section 3.3). There are two main considerations: (1) whether the same molecular populations are accessed in measurements on cavities (**C** samples) as compared to a general molecular population in **T** samples and (2) how the presence of polaritons might alter excited-state dynamics relevant for photodimerization. In particular:

1) Because photodimerization efficiency in the solid state strongly relies on the availability of intermolecular orientations satisfying the geometrical constraint for the

https://doi.org/10.1021/acs.jpcc.1c06881
J. Phys. Chem. C 2021, 125, 27072−27083

photodimerization process, it is conceivable that cavity selectively couples to particular domains (maximizing the alignment between the molecular transition dipole moments and the cavity electric field) which satisfy similar requirements. In this case, in **C** samples, only a subset of a general population of degrading molecules seen in **T** samples, which is more conducive to photodimerization, would be observed by measuring polariton properties of Figures 6 and 7. In our previous work on functionalized anthradithiophene- and pentacene-based polycrystalline films in cavities,[18,47] we have observed preferential cavity coupling to particular molecular populations (namely, to amorphous phases in the mixed-phase films with coexisting amorphous and crystalline domains). The TIPS-Tc films in the present study, however, are amorphous, and so a preferential cavity coupling to domains with a particular local nanoenvironment conducive for photodimerization would be harder to envision, although it cannot be excluded.

2) The most relevant considerations pertaining to excited-state dynamics are (i) whether the ultrashort-lived (<100 fs in our low-Q cavities) polariton states themselves could cause an ultrafast dimerization and (ii) how the mixing of polariton states with various dark states discussed in the literature[24,48,49] could promote dimerization. (Here, "dark" states refer to molecular states that are not coupled to the cavity photon but still coexist with polariton states.) Although ultrafast dimerization has been documented,[50] it requires special conditions (for example, the presence of conical intersection between the ground and first excited states along the cycloaddition pathway in the case of sub-ps thymine dimerization[51]), the existence of which is highly unlikely for TIPS-Tc. Thus, we discard the consideration (i). The mixing between coherent polariton states and incoherent dark states (consideration (ii)) and establishment of a quasi-equilibrium between polariton states such as LP and dark states has been recently discussed in a context of photochemistry.[48] For example, ref 48 argued that low entropy of polariton states may lead to a higher free energy, as compared to that of dark states, even with the lower electronic energy of a polariton state (e.g., the LP energy in all **C** samples is lower than that of the S_1 exciton). The high free energy then may enable populating dark states even from a LP state and initiate dark state-mediated photochemical reactions upon LP excitation. Applying this logic to our case, the enhanced reactivity would be expected if polariton state−dark state mixing could promote routing of the excited-state population into the states responsible for dimerization. Polariton states have been shown to effectively harvest populations from excited states of various multiplicity.[24,49] For example, the population of the LP state from a ^{5}(TT) state has been observed in TIPS-Tc cavities,[24] resulting in an enhanced delayed PL emission. Notably, this effect was only weakly dependent upon cavity detuning, similar to our observations of weak-cavity detuning-dependent dimerization rates in Section 3.3. If mixing with polariton states promotes transfer of some of the ^{5}(TT) population to the ^{1}(TT) and/or the S_1 states (whose role in dimerization was discussed above), this could promote reactivity. For example, in contrast to the ^{5}(TT) state, the ^{1}(TT) state could regenerate the S_1 state (which is responsible for "butterfly" dimerization in "bare" films)[34] or provide the kinetic advantage for the T_1 state generation (toward alkyne dimerization).

In addition to thermodynamics, the overall excited-state kinetics could also play a role. It has been shown theoretically[52] that the TT state formation kinetics in strongly cavity-coupled organic aggregates is affected by the interplay between the intermolecular interactions and the cavity coupling, and it could be made considerably faster in a cavity-coupled aggregate as compared to a "bare" aggregate. This may promote, for example, the alkyne dimerization if the faster TT formation also translates into a faster TT dissociation into free triplets T_1. However, further studies are necessary to establish which, of all factors discussed above, is dominant in the cavity-enhanced photodimerization.

5. CONCLUSIONS

In summary, we observed distinct photodegradation mechanisms in TIPS-Tc films in the presence and absence of oxygen, with the quantum yields for the associated reactions differing by more than two orders of magnitude, but in both cases enhanced for molecular configurations favoring the TT state formation and their immediate surroundings. Alkyne dimer formation was identified as an oxygen-independent reaction pathway responsible for up to 34% of TIPS-Tc photoconversion upon continuous 532 nm irradiation. Under strong coupling conditions, the reaction rate was enhanced by a factor of ∼4.2 in resonant cavities as compared to the "bare" TIPS-Tc films, with the enhancement robust with respect to cavity detuning. We expect that findings discussed here would be relevant for a large class of high-performance functionalized acene derivatives, particularly those that undergo singlet fission. The ability to manipulate photochemical reactivity in these materials by cavity coupling represents an opportunity to learn how to control these technologically relevant reactions and to understand fundamental properties of polariton states and their participation in chemical reactions.

■ ASSOCIATED CONTENT

Supporting Information

The Supporting Information is available free of charge at https://pubs.acs.org/doi/10.1021/acs.jpcc.1c06881.

Details of sample preparation, experimental and data fitting protocols, optical characterization of films and cavities, PL spectra and lifetimes, photodegradation rate extraction for various samples, cavity data modeling details, DFT results for TIPS-Tc, Tc-EPO, and alkyne dimers, and photodegradation data for cavities with various detunings (PDF)

■ AUTHOR INFORMATION

Corresponding Author

Oksana Ostroverkhova − *Department of Physics, Oregon State University, Corvallis, Oregon 97331, United States;* orcid.org/0000-0002-3833-161X; Email: oksana@science.oregonstate.edu

Authors

Richard Puro − *Department of Physics, Oregon State University, Corvallis, Oregon 97331, United States*

Jonathan D. B. Van Schenck − *Department of Physics, Oregon State University, Corvallis, Oregon 97331, United States*
Reid Center − *Department of Physics, Oregon State University, Corvallis, Oregon 97331, United States*
Emma K. Holland − *Center for Applied Energy Research, University of Kentucky, Lexington, Kentucky 40511, United States*
John E. Anthony − *Center for Applied Energy Research, University of Kentucky, Lexington, Kentucky 40511, United States;* orcid.org/0000-0002-8972-1888

Complete contact information is available at: https://pubs.acs.org/10.1021/acs.jpcc.1c06881

Notes

The authors declare no competing financial interest.

■ ACKNOWLEDGMENTS

This work was supported by the National Science Foundation (CHE-1956431 to O.O. and Cooperative Agreement No. 1849213 to J.E.A.). The sample fabrication was made possible through facilities supported by the NSF NNCI:NNI EECS-2025489 award.

■ REFERENCES

(1) Ostroverkhova, O. Organic Optoelectronic Materials : Mechanisms and Applications. *Chem. Rev.* **2016**, *116*, 13279−13412.
(2) Ostroverkhova, O. *Handbook of Organic Materials for Electronic and Photonic Devices* 2nd Ed., Elsevier, 2018.
(3) Hertzog, M.; Wang, M.; Mony, J.; Borjesson, K. Strong Light − Matter Interactions : A New Direction within Chemistry. *Chem. Soc. Rev.* **2019**, *48*, 937−961.
(4) Herrera, F.; Owrutsky, J. Molecular Polaritons for Controlling Chemistry with Quantum Optics. *J. Chem. Phys.* **2020**, *152*, 100902.
(5) Du, M.; Ribeiro, R. F.; Yuen-Zhou, J. Remote Control of Chemistry in Optical Cavities. *Chem* **2019**, *5*, 1167−1181.
(6) Kena-Cohen, S.; Yuen-Zhou, J. Polariton Chemistry: Action in the Dark. *ACS Cent. Sci.* **2019**, *5*, 386−388.
(7) Ribeiro, R. F.; Mart, L. A.; Du, M.; Campos-Gonzalez-Angulo, J.; Yuen-Zhou, J. Polariton Chemistry : Controlling Molecular Dynamics with Optical Cavities. *Chem. Sci.* **2018**, *9*, 6325−6339.
(8) Galego, J.; Garcia-Vidal, F. J.; Feist, J. Suppressing Photochemical Reactions With Quantized Light Fields. *Nat. Commun.* **2016**, *7*, 13841.
(9) Herrera, F.; Spano, F. C. Cavity-Controlled Chemistry in Molecular Ensembles. *Phys. Rev. Lett.* **2016**, *116*, No. 238301.
(10) Hutchison, J. A.; Schwartz, T.; Genet, C.; Devaux, E.; Ebbesen, T. W. Modifying Chemical Landscapes by Coupling to Vacuum Fields. *Angew. Chem., Int. Ed.* **2012**, *51*, 1592−1596.
(11) Thomas, A.; Lethuillier-Karl, L.; Nagarajan, K.; Vergauwe, R. M. A.; George, J.; Chervy, T.; Shalabney, A.; Devaux, E.; Genet, C.; Moran, J.; et al. Tilting a Ground-State Reactivity Landscape by Vibrational Strong Coupling. *Science* **2019**, *363*, 615−619.
(12) Munkhbat, B.; Wersäll, M.; Baranov, D. G.; Antosiewicz, T. J.; Shegai, T. Suppression of Photo-Oxidation of Organic Chromophores by Strong Coupling to Plasmonic Nanoantennas. *Sci. Adv.* **2018**, *4*, No. eaas9552.
(13) Mony, J.; Climent, C.; Petersen, A. U.; Moth-Poulsen, K.; Feist, J.; Börjesson, K. Photoisomerization Efficiency of a Solar Thermal Fuel in the Strong Coupling Regime. *Adv. Funct. Mater.* **2021**, *31*, No. 2010737.
(14) Peters, V.; Faruk, M.; Asane, J.; Alexander, R.; Peters, D.; Prayakarao, S.; Rout, S.; Noginov, M. Effect of Strong Coupling on Photodegradation of the Semiconducting Polymer P3HT. *Optica* **2019**, *6*, 318.
(15) Kena-Cohen, S.; Forrest, S. R. Giant Davydov Splitting of the Lower Polariton Branch in a Polycrystalline Tetracene Microcavity. *Phys. Rev. B* **2008**, *77*, No. 073205.
(16) Kéna-Cohen, S.; Davanço, M.; Forrest, S. Strong Exciton-Photon Coupling in an Organic Single Crystal Microcavity. *Phys. Rev. Lett.* **2008**, *101*, No. 116401.
(17) Liu, B.; Menon, V. M.; Sfeir, M. Y. The Role of Long-Lived Excitons in the Dynamics of Strongly Coupled Molecular Polaritons. *ACS Photonics* **2020**, *7*, 2292−2301.
(18) Van Schenck, J.; Tanyi, E.; Cheng, L.-J.; Anthony, J.; Ostroverkhova, O. Strong Exciton−Photon Coupling in Anthradithiophene Microcavities: From Isolated Molecules to Aggregates. *MRS Commun.* **2019**, *3*, 956−963.
(19) Kena-Cohen, S.; Forrest, S. R. Room-Temperature Polariton Lasing in an Organic Single-Crystal Microcavity. *Nat. Photonics* **2010**, *4*, 371−375.
(20) Stern, H. L.; Musser, A. J.; Gelinas, S.; Parkinson, P.; Herz, L. M.; Bruzek, M. J.; Anthony, J.; Friend, R. H.; Walker, B. J. Identification of a Triplet Pair Intermediate in Singlet Exciton Fission in Solution. *Proc. Natl. Acad. Sci.* **2015**, *112*, 7656−7661.
(21) Dover, C. B.; Gallaher, J. K.; Frazer, L.; Tapping, P. C.; Ii, A. J. P.; Crossley, M. J.; Anthony, J. E.; Kee, T. W.; Schmidt, T. W. Endothermic Singlet Fission Is Hindered by Excimer Formation. *Nat. Chem.* **2018**, *10*, 305.
(22) Stern, H. L.; Cheminal, A.; Yost, S. R.; Broch, K.; Bayliss, S. L.; Chen, K.; Tabachnyk, M.; Thorley, K.; Greenham, N.; Hodgkiss, J. M.; et al. Vibronically Coherent Ultrafast Triplet-Pair Formation and Subsequent Thermally Activated Dissociation Control Efficient Endothermic Singlet Fission. *Nat. Chem.* **2017**, *9*, 1205−1212.
(23) Miyata, K.; Conrad-burton, F. S.; Geyer, F. L.; Zhu, X. Triplet Pair States in Singlet Fission. *Chem. Rev.* **2019**, *119*, 4261−4292.
(24) Polak, D.; Jayaprakash, R.; Lyons, T. P.; Martínez-Martínez, L. Á.; Leventis, A.; Fallon, K. J.; Coulthard, H.; Bossanyi, D. G.; Georgiou, K.; Petty, A. J., II; Anthony, J.; Bronstein, H.; Yuen-Zhou, J.; Tartakovskii, A. I.; Clark, J.; Musser, A. J. Manipulating Molecules with Strong Coupling : Harvesting Triplet Excitons in Organic Exciton Microcavities. *Chem. Sci.* **2020**, *11*, 343−354.
(25) Fudickar, W.; Linker, T. Why Triple Bonds Protect Acenes from Oxidation and Decomposition. *J. Am. Chem. Soc.* **2012**, *134*, 15071−15082.
(26) Van Schenck, J. D. B.; Mayonado, G.; Anthony, J. E.; Graham, M.; Ostroverkhova, O. Molecular Packing-Dependent Exciton Dynamics in Functionalized Anthradithiophene Derivatives: From Solutions to Crystals. *J. Chem. Phys.* **2020**, *153*, 164715.
(27) Van Schenck, J. D. B.; Giesbers, G.; Kannegulla, A.; Cheng, L.-J.; Anthony, J. E.; Ostroverkhova, O. Molecular Packing-Dependent Exciton and Polariton Dynamics in Anthradithiophene Organic Crystals. *MRS Adv.* **2018**, *3*, 3465−3470.
(28) Giesbers, G.; Van Schenck, J.; Quinn, A.; Van Court, R.; Gutierrez, S.; Robinson, S.; Ostroverkhova, O. Xylindein: Naturally Produced Fungal Compound for Sustainable (Opto)Electronics. *ACS Omega* **2019**, *4*, 13309−13318.
(29) Coppo, P.; Yeates, S. G. Shining Light on a Pentacene Derivative: The Role of Photoinduced Cycloadditions. *Adv. Mater.* **2005**, *17*, 3001−3005.
(30) Guerzo, D.; Pozzo, J.; Desvergne, J.; Olive, A. G. L. Photodimerization of Soluble Tetracene Derivatives Using Visible Light. *J. Phys. Org. Chem.* **2007**, *20*, 838−844.
(31) Bouas-laurent, H.; Castellan, A.; Desvergne, J.; Lapouyade, R. Photodimerization of Anthracenes in Fluid Solution : Structural Aspects. *Chem. Soc. Rev.* **2000**, *29*, 43−55.
(32) Tong, F.; Hanson, M. P.; Bardeen, C. J. Analysis of Reaction Kinetics in the Photomechanical Molecular Crystal 9-Methylanthracene Using an Extended Finke−Watzky Model. *Phys. Chem. Chem. Phys.* **2016**, *18*, 31936−31945.
(33) Dong, S.; Ong, A.; Chi, C. Photochemistry of Various Acene Based Molecules. *J. Photochem. Photobiol. C* **2019**, *38*, 27−46.
(34) Charlton, J. L.; Dabestani, R.; Saltiel, J. Role of Triplet-Triplet Annihilation in Anthracene Dimerization1a. *J. Am. Chem. Soc.* **1983**, *105*, 3473−3476.
(35) Zade, S. S.; Zamoshchik, N.; Reddy, A. R.; Fridman-Marueli, G.; Sheberla, D.; Bendikov, M. Products and Mechanism of Acene

Dimerization. A Computational Study. *J. Am. Chem. Soc.* **2011**, *133*, 10803−10816.
(36) Morě, R.; Busse, G.; Hallmann, J.; Paulmann, C.; Scholz, M.; Techert, S. Photodimerization of Crystalline 9-Anthracenecarboxylic Acid: A Nontopotactic Autocatalytic Transformation. *J. Phys. Chem. C* **2010**, *114*, 4142−4148.
(37) Purushothaman, B.; Parkin, S. R.; Anthony, J. E. Synthesis and Stability of Soluble Hexacenes. *Org. Lett.* **2010**, *12*, 2060−2063.
(38) Payne, M. M.; Odom, S. A.; Parkin, S. R.; Anthony, J. E. Stable, Crystalline Acenedithiophenes with up to Seven Linearly Fused Rings. *Org. Lett.* **2004**, *6*, 3325−3328.
(39) Easley, C. J.; Tong, F.; Dong, X.; Al-Kaysi, R. O.; Bardeen, C. J. Using Light Intensity to Control Reaction Kinetics and Reversibility in Photomechanical Crystals. *Chem. Sci.* **2020**, *11*, 9852−9862.
(40) Spano, F. C. Optical Microcavities Enhance the Exciton Coherence Length and Eliminate Vibronic Coupling in J-Aggregates. *J. Chem. Phys.* **2015**, *142*, 184707.
(41) Long, Y. Improving Optical Performance of Inverted Organic Solar Cells by Microcavity Effect. *Appl. Phys. Lett.* **2009**, *95*, 48−51.
(42) Dodabalapur, A.; Rothberg, L. J.; Jordan, R. H.; Miller, T. M.; Slusher, R. E.; Phillips, J. M. Physics and Applications of Organic Microcavity Light Emitting Diodes. *J. Appl. Phys.* **1996**, *80*, 6954−6964.
(43) Dabestani, R.; Nelson, M.; Sigman, M. E. Photochemistry of Tetracene Adsorbed on Dry Silica: Products and Mechanism. *Photochem. Photobiol.* **1996**, *64*, 80−86.
(44) Shoaee, S.; Durrant, J. R. Oxygen Diffusion Dynamics in Organic Semiconductor Films. *J. Mater. Chem. C* **2015**, *3*, 10079−10084.
(45) Nonell, S.; Flors, C. *Singlet Oxygen: Applications in Biosciences and Nanosciences*; RSC Publishing, 2016.
(46) Ajaz, A.; Bradley, A. Z.; Burrell, R. C.; Li, W. H. H.; Daoust, K. J.; Bovee, L. B.; DiRico, K. J.; Johnson, R. P. Concerted vs Stepwise Mechanisms in Dehydro-Diels−Alder Reactions. *J. Org. Chem.* **2011**, *76*, 9320−9328.
(47) Van Schenck, J. D. B.; Goldthwaite, W.; Puro, R.; Anthony, J. E.; Ostroverkhova, O. Exciton Polaritons Reveal "Hidden" Populations in Functionalized Pentacene Films. *J. Phys. Chem. C*, **2021**, in press, DOI: 10.1021/acs.jpcc.1c08257.
(48) Scholes, G. D.; Delpo, C. A.; Kudisch, B. Entropy Reorders Polariton States. *J. Phys. Chem. Lett.* **2020**, *11*, 6389−6395.
(49) Berghuis, A. M.; Halpin, A.; Le-van, Q.; Ramezani, M.; Wang, S.; Murai, S.; Rivas, J. G. Enhanced Delayed Fluorescence in Tetracene Crystals by Strong Light-Matter Coupling. *Adv. Funct. Mater.* **2019**, *29*, No. 1901317.
(50) Schreier, W. J.; Schrader, T. E.; Koller, F. O.; Gilch, P.; Crespo-Hernández, C. E.; Swaminathan, V. N.; Carell, T.; Zinth, W.; Kohler, B. Thymine Dimerization in DNA Is an Ultrafast Photoreaction. *Science* **2007**, *315*, 625−629.
(51) Boggio-Pasqua, M.; Groenhof, G.; Schäfer, L. V.; Grubmüller, H.; Robb, M. A. Ultrafast Deactivation Channel for Thymine Dimerization. *J. Am. Chem. Soc.* **2007**, *129*, 10996−10997.
(52) Zhang, B.; Zhao, Y.; Liang, W. Z. Joint Effects of Exciton-Exciton and Exciton-Photon Couplings on the Singlet Fission Dynamics in Organic Aggregates. *J. Phys. Chem. C* **2021**, *125*, 1654−1664.

https://doi.org/10.1021/acs.jpcc.1c06881
J. Phys. Chem. C 2021, 125, 27072−27083